

## Molecular movie for the isomerization of acetylene dication made by time resolved Coulomb imaging

Zheng Li<sup>1,2,3,\*</sup>, Ludger Inhester<sup>2,3</sup>, Basile Curchod<sup>4</sup>, Chelsea Liekhus-Schmaltz<sup>1,5</sup>, Oriol Vendrell<sup>2,3</sup>, Nikita Medvedev<sup>2,3</sup>, Stefan Pabst<sup>6</sup>, James Cryan<sup>1</sup>, Timur Osipov<sup>1</sup>, Phil Bucksbaum<sup>1,5</sup>, Todd Martinez<sup>1,4,†</sup>

<sup>1</sup>SLAC National Accelerator Laboratory, 2575 Sand Hill Road, Menlo Park, CA 94025, USA

<sup>2</sup>Center for Free Electron Laser Science, Deutsches Elektronen-Synchrotron,  
Notkestraße 85, D-22607 Hamburg, Germany

<sup>3</sup>Hamburg Center for Ultrafast Imaging, Luruper Chaussee 149, D-22761 Hamburg, Germany

<sup>4</sup>Department of Chemistry, Stanford University, 333 Campus Drive, Stanford, CA 94305, USA

<sup>5</sup>Department of Physics, Stanford University, 382 Via Pueblo Mall, Stanford, CA 94305, USA

<sup>6</sup>Harvard-Smithsonian Center for Astrophysics, 60 Garden Street, Cambridge, MA 02138, USA

Experimental evidence has pointed toward the existence of ultrafast proton migration and isomerization as a key process for acetylene and its ions, however the actual mechanism for ultrafast isomerization of the acetylene  $[\text{HCCH}]^{2+}$  to vinylidene  $[\text{H}_2\text{CC}]^{2+}$  dication remains nebulous. Theoretical studies show a high potential barrier of over 2 eV [J. Chem. Phys. 123, 134320 (2005)] for the isomerization pathways on the low lying dicationic states, the corresponding isomerization should take picoseconds. However a recent experiment with femtosecond X-ray free electron laser (XFEL) [Nature Commun. 6, 8199 (2015)] suggests signature of isomerization proceeding on a sub-100 femtosecond time scale. We present here a complete theoretical study of the dynamics of acetylene dication from Auger decay induced by X-ray photoionizing the carbon K shell. We find a pathway from high lying dissociative dicationic states, which can lead to the sub-100fs isomerization with assistance of the non-Born-Oppenheimer effect. Moreover, our study points out the decisive role of non-Born-Oppenheimer effect, without which the ultrafast isomerization may not be possible. The study resolves a long-standing puzzle of a seemingly contradiction between experiment and theory concerning the time scale of isomerization.

PACS numbers: 33.80.Eh,

The vinylidene geometry is an important intermediate geometry in many reactions involving  $\text{C}_2\text{H}_2$ . However, unlike in the neutral and cationic species [1-5], the pathway to isomerization of the acetylene dication from  $[\text{HCCH}]^{2+}$  to  $[\text{H}_2\text{CC}]^{2+}$  remains largely unresolved. The reason for this disparity is an apparent contradiction between theory and experimental observation which has prompted numerous studies [6-13]. Arguments from both sides can be summed up as follows. Experimental synchrotron data concludes that isomerization occurs on the low lying dicationic states  $^1\Sigma_g$  and  $^1\Delta_g$  with vacancies  $1\pi_u^{-2}$ , while deprotonation and symmetric breakup occur on the higher lying  $^1\Pi_u$  states with  $1\pi_u^{-1}3\sigma_g^{-1}$  character [7,

14]. In addition photoelectron-photoion momentum spectroscopy [6, 7] and more recent time-resolved Coulomb imaging [10] experiments suggest that ultrafast hydrogen migration occurs under 100 fs. A third separate FEL experiment at LCLS proves the existence of significant hydrogen migration in under 100 fs. These three pieces of evidence would seem to conclude that isomerization proceeds on the low lying dicationic states on a sub-100 fs time scale.

Contrary to this evidence, *ab initio* electronic structure calculations suggest a barrier of  $\sim 2\text{eV}$  on the double hole states  $1\pi_u^{-2}$  for isomerization [8, 9], to cross this barrier and isomerize should take picoseconds, which is orders of magnitude different than the 100 fs observed. One possible solution to this difference between theory and experiment is that while true isomerization is indeed occurring on the low lying dication states, significant proton migration is occurring on higher lying states before deprotonation or symmetric breakup.

In the higher lying  $1\pi_u^{-1}3\sigma_g^{-1}$  states of the dication proton migration is not limited by a barrier, however the double valence hole in these states weakens the C-C bond. The C-C bond length of the dication therefore relaxes from  $1.21\text{\AA}$  to  $1.37\text{\AA}$ , resulting in a relaxation energy of  $\sim 2.4\text{ eV}$ . Such a weak C-C bond makes it very difficult to maintain a bound  $[\text{C}_2\text{H}_2]^{2+}$  structure before the proton migrates from one carbon atom to another, instead the  $\text{CH}^+ + \text{CH}^+$  channel should be overwhelming. However, because there is significant migration before the breakup is completed, proton migration will be detected in the time resolved x-ray experiment. As well, since breakup occurs in under 100 fs, when the second x-ray pulse comes after break up, the two fragments have a chance to rotate relative to one another, causing it to appear as though isomerization is completing. This process largely reproduces the deuteron migration signal seen in this experiment.

While this can explain the major signal seen in this experiment, we have identified an unusual sub-100 fs isomerization pathway that starts from a highly dissociative  $1\pi_u^{-1}3\sigma_g^{-1}$  state and ends up with an isomerized  $[\text{CH}_2\text{C}]^{2+}$  on a  $1\pi_u^{-2}$  state with an estimated branching ratio of  $2.5 \times 10^{-4}$  compared to the symmetric breakup from rate theory [15]. The key ingredient of this ultrafast isomerization pathway is the combined characters of a freely roaming proton on the  $1\pi_u^{-1}3\sigma_g^{-1}$  state and a stronger C-C bond on the  $1\pi_u^{-2}$ . The only known link of these two characters is through the non-Born-Oppenheimer effect that builds the tunnels between these states.

Here we present a complete time-resolved picture of XFEL induced acetylene dication dynamics with theoretical simulation of the X-ray photoionization. We model the dynamics of the core-ionized cation and its Auger decay and the dynamics of the dication, as well as the momenta distribution in the time resolved Coulomb imaging that was used to record a molecular movie for the dynamics of  $\text{C}_2\text{H}_2^{2+}$  as

shown in Fig. 1.

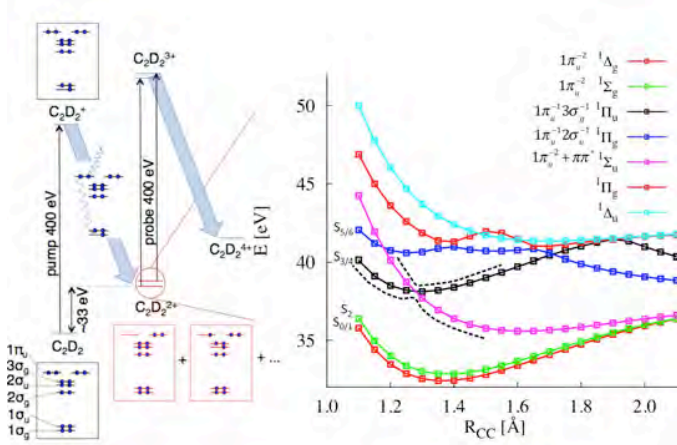


FIG. 1. Sketch of the acetylene dication dynamics induced by X-ray photoionization and Auger decay. A second X-ray pulse with a variable delay further core ionizes the dication and creates the Coulomb momenta mapping as described in the text. The potential curves of the singlet dicationic states are plotted in the adiabatic representation, their diabatic electronic characters are given in Fig. S1 (see supplementary material[15]). The first 3 adiabatic states  $S_0$ - $S_2$  have dominant character of double hole configuration  $1\pi_u^{-2}$ , and higher lying states  $S_3$ ,  $S_4$  are characterized by double hole configuration  $1\pi_u^{-1}3\sigma_g^{-1}$ , with electron hole in both  $\pi$ - and  $\sigma$ -orbitals. The black dashed lines label the barrierless fragmentation passage of  $S_3$  state formed by crossing of diabatic states  ${}^1\Pi_u(1\pi_u^{-1}3\sigma_g^{-1})$  and  ${}^1\Sigma_u(1\pi_u^{-2} + \pi_u-\pi_g^*)$ .

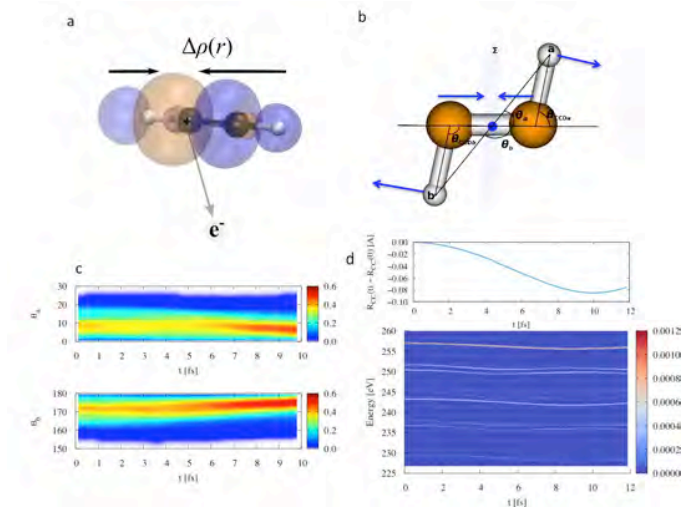


FIG. 2. Dynamics of the core ionized acetylene cation. (a) The relaxed electron density  $\rho_{-1}(r)$  after carbon  $K$  edge photoionization.  $\Delta\rho(r) = \rho_{-1}(r) - \tilde{\rho}_{-1}(r)$  is shown, where  $\tilde{\rho}_{-1}(r)$  is the electron density of unrelaxed core hole state by removing one electron from  $C1s$  orbital. (b) characteristic motion of cation, C-C bond contraction and CCD linearization. (c) Evolution of angles  $\theta_a$  and  $\theta_b$  shows the cation evolves towards linear structure. (d) The time-resolved Auger spectra from a representative

trajectory and the evolution of C-C bond length and total kinetic energy of the cation before Auger decay, the contracting C-C bond results in red shift in Auger electron energies. The Lorentzian broadening due to lifetime of the core-hole state is included to the Auger spectra.

In our simulation, we adopt  $C_2D_2^+$  rather than  $C_2H_2^+$ , in order to have a faithful reproduction of the experimental scenario, where the deuterated acetylene was employed to eliminate potential background sources of protons from water and other contaminants[10]. Although the deuterated acetylene should have the same electronic structure except for second order Born-Huang coupling which is negligible in our scenario, the particle velocity and the rate of the tunneling through the barrier are expected to be slower in  $C_2D_2^+$  compared with  $C_2H_2^+$ . However, experiment shows clear signature of vinylidene-like channel already in the first 12 fs following core ionization[10]. The X-ray induced dynamics starts from photoionization in the carbon  $K$  shell. In order to describe the dynamics of the core ionized cation on  $^2\Sigma$  state, we adopt a  $\Delta$ SCF scheme with a maximum overlap method[15, 16]. For the modelling of the core hole state we adopt a localized hole picture describing a core hole on one carbon atom. As shown in Fig. 1(a), the dynamics screening of core hole through shake-up process enhances the valence electron density in the C-C bond region. The electron reorganization strengthens the bonding along the molecular axis, and hardens the angular potential for the deuteron atom along the  $\theta_{CCD}$  coordinate[15]. Using this electronic structure model, we carried out *ab initio* molecular dynamics simulation of core ionized acetylene cation with initial conditions reflecting the vibrational ground state Wigner distribution of the neutral acetylene.

Fig. 2(c) and (d) present the evolution of the angular distribution of the deuteron atoms and the C-C distance from dynamics in the cationic  $^2\Sigma$  state. The nuclear dynamics after core ionization can be mainly characterized by a contraction of the C-C bond and a formation of a generally more linear geometry. Along the trajectory the instantaneous Auger spectra is computed (see Fig. 2(d))[15, 17]. The electronic energy of the final states after Auger decay is lowered, because the C-C bond length decreases due to C-C contraction in the cationic  $^2\Sigma$  state, and the resulting dicationic states from Auger decay should have higher energy due to Coulomb repulsion between the double hole that become closer to each other. Thus the energy difference between the core ionized state and the repulsive dicationic final state decreases along the C-C contraction. This effect leads to a redshifted Auger spectrum as the dynamics proceeds. From the time-resolved Auger spectrum along cationic trajectories, we populate the first five singlet dicationic states and first three triplet states with probabilities derived from the decay rate of the  $K$  shell core hole state  $|K\rangle$  to different dicationic states  $|LL\rangle$  with double hole in  $L$ -shell as  $P_{KLL_i} = \rho_K(t)\Gamma_{KLL_i}(t)\Delta t$ , where  $\Gamma_{KLL_i}(t)$  is the Auger rate at a delay time of  $t$  after  $C1s$  core ionization and  $\rho_K(t)$  is the population the core ionized state determined by the kinetic rate equation  $\dot{\rho}_K(t) = -\rho_K(t)\Gamma(t)$ ,  $\rho_K(0) = 1$ , where  $\Gamma(t) = \sum_{|KLL_i\rangle} \Gamma_{KLL_i}(t)$  is the

total Auger rate. We assume that the initial positions and momenta of the dication are inherited from the parent cation at the time of Auger decay and a recoil momentum from Auger electron is added on the carbon atom subject to primary core-ionization. In the following discussion, we focus on the lowest five singlet and three triplet dicationic states. The higher lying states are not of relevance here because they are found to be too dissociative to support isomerization, which requires a bounded structure to allow proton to migrate between carbon atoms. Thus higher lying states will result in either symmetric breaking  $\text{CH}^+ + \text{CH}^+$  or deprotonation  $\text{C}_2\text{H}^+ + \text{H}^+$  channels. Besides, Auger rate for decaying into triplet states that are supportive for isomerization are one order of magnitude lower than that of dominant singlet states. Generally the acetylene cation decays into  $\text{C}_2\text{H}_2^{2+}$  dication with an Auger lifetime of  $\sim 8$  fs.

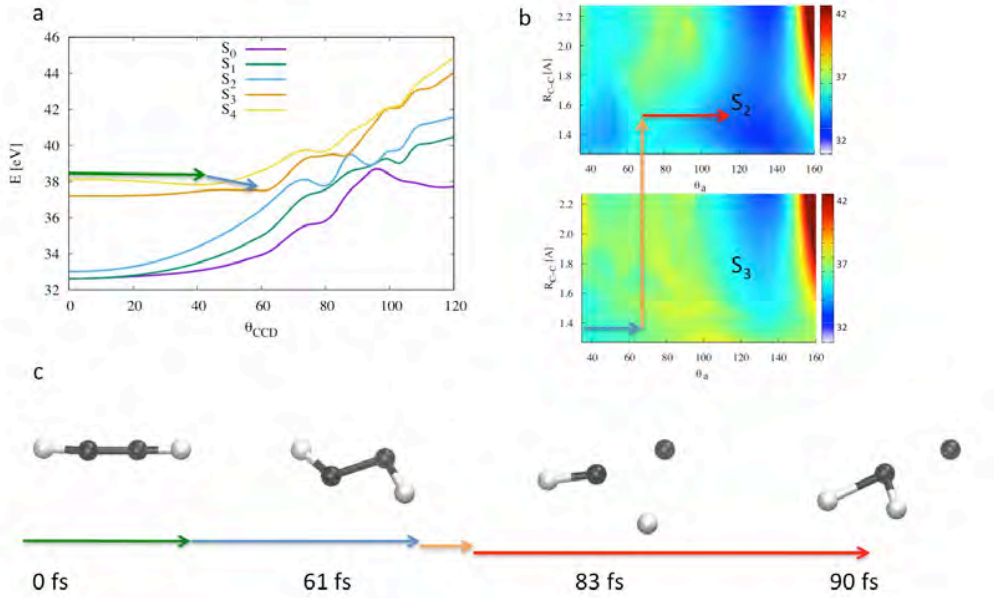


FIG. 3. A schematic description of the sub-100 fs isomerization pathway. The trajectory (c) starts from the high lying  $1\pi_u^{-1}3\sigma_g^{-1}$  states  $S_4$  (a) that allows the deuteron atom to move to a large angle before 60 fs, the non-Born-Oppenheimer transition downwards to  $S_3$  and  $S_2$  offers a bounded potential for the C-C bond (b), the dication then isomerizes on the low lying  $1\pi_u^{-2}$  states at ca. 90 fs. In (a) the potentials are calculated with  $R_{\text{CD}} = 1.12 \text{ \AA}$ ,  $R_{\text{CC}} = 1.37 \text{ \AA}$  and trans-bending angle  $\theta_{\text{CCD}}$ , in (b) they are calculated with  $R_{\text{CM-D}} = 1.49 \text{ \AA}$ ,  $R_{\text{CC}} = 1.37 \text{ \AA}$ , and deuteron migration angle  $\theta_a$ ,  $R_{\text{CM-D}}$  is the distance of the migrating hydrogen to the center of mass (CM) of the two carbon atoms, and we define  $\theta_a = \theta_{\text{C-CM-D}}$ . The arrow in (a) illustrates the direction of the isomerization, and the arrow in (b) shows the pathway of electronic decay through the conical intersection from  $S_3$  to  $S_2$  that occur at the end of the isomerization process.

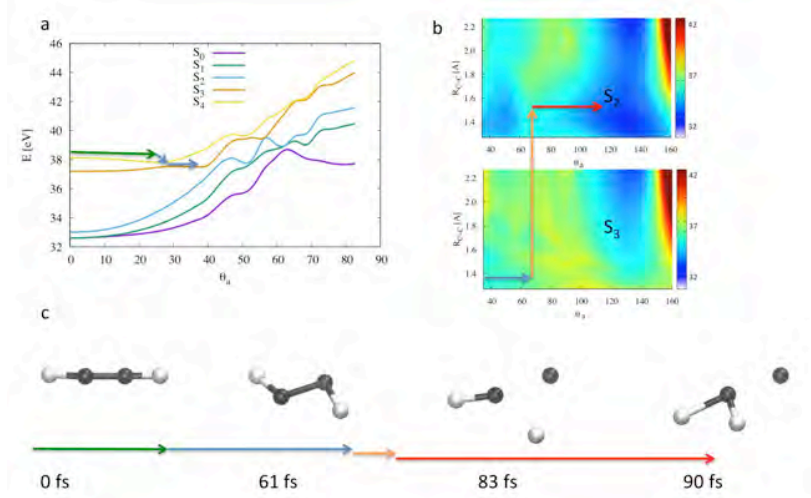


Fig. 3-1. (a) trans-bending potential plotted with  $\theta_a$  coordinate and assume  $\theta_b = \pi + \theta_a$ .

We now focus on the dication dynamics initiated after Auger decay, and explore the possibility of isomerization within 100 fs. The molecular dynamics on the dicationic states are described with the mixed quantum-classical fewest-switches surface hopping method[18], the electronic structure is solved on a complete active space self-consistent field theory level at each time step, and corresponding potential energies, gradients and non-Born-Oppenheimer couplings necessary for the classical evolution of the nuclear coordinates and quantum evolution of the electronic degrees of freedom are computed on the fly[2, 3, 19]. For each trajectory of the fewest-switches surface hopping ensemble the amplitude of each electronic eigenstate is integrated in time according to the Schrödinger equation

$$i\hbar\dot{A}_l(t) = \sum_m H_{lm}(R(t), \dot{R}(t))A_m(t) \quad (1.1)$$

where  $H_{lm}$  is a matrix element of the effective time-dependent Hamiltonian for the evolution of the electronic subsystem along the corresponding classical nuclear trajectory, its diagonal elements correspond to the adiabatic electronic potential  $V_l(R)$ , and the off-diagonal elements contain the nonadiabatic couplings  $-i\hbar\dot{R} \cdot \langle \Psi_l^{N-2} | \nabla_R | \Psi_m^{N-2} \rangle$  between dicationic electronic states with  $N-2$  electrons. The electronic wave packet propagated along each nuclear trajectory hence reads  $|\Psi(t)\rangle = \sum_l A_l(t) |\Psi_l^{N-2}\rangle$ . The ensemble of nuclear trajectories represents a classical approximation of the time evolution of the corresponding quantum wave packet.

As shown in Fig. 3(a), the low lying  $1\pi_u^{-2}$  states have high barrier for the trans-bending motion of dication. For the  $1\pi_u^{-1}3\sigma_g^{-1}$  states, the trans-bending motion is barrier free until  $\sim 60^\circ$ . The difference of trans-bending barrier heights of  $1\pi_u^{-2}$  and  $1\pi_u^{-1}3\sigma_g^{-1}$  states can be understood from types of the bonding. The  $\sigma$ -bond is unidirectional along the C-C axis, and favors a linear C-C-D structure. Thus only by removing electron from a bonding  $\sigma$ -orbital and weakening the  $\sigma$ -bond, the deuterons can have more freedom to rapidly move to a higher  $\theta_{CCD}$  angle. Thus it is

possible on the  $1\pi_u^{-1}3\sigma_g^{-1}$  states to have a large angle bending along  $\theta_{\text{CCD}}$  angle on sub-100 fs scale. In contrast, the high barrier of the lowest three  $1\pi_u^{-2}$  states implies that the effective trans-bending motion that leads to isomerization on these states should take several picoseconds. However, for the high lying  $1\pi_u^{-1}3\sigma_g^{-1}$  states, there is a very low barrier along C-C stretch (see Fig. 3(b)), the dication is prone to dissociate rather than isomerize. Generally, we should expect the isomerization to be a rare channel with low branching ratio to the symmetric breaking or deprotonation channels. In Fig. S6, we show the  $(\theta_{\text{CCD}}, R_{\text{CC}})$  accessed by 1200 molecular dynamics trajectories, no isomerization channel was detected, since the deuteron atoms reside on the same side of the bisection plane dividing the C-C axis[15].

Because the non-Born-Oppenheimer coupling allows transition between electronic states induced by nuclear motion[2, 3, 19], the dication can undergo proton migrating half way between the carbon atoms with a large  $\theta_{\text{CCD}}$  angle on the  $1\pi_u^{-1}3\sigma_g^{-1}$  states with soft angular potential, and make transition downwards to the  $1\pi_u^{-2}$  states to complete isomerization on the  $1\pi_u^{-2}$  states with bounded potential along C-C stretch coordinate. Such a trajectory is shown in Fig. 3(c) with the trans-bending motion to  $\theta_{\text{CCD}}$  angle of  $\sim 80^\circ$  within 60 fs on the state  $S_4$  and  $S_3$  with  $1\pi_u^{-1}3\sigma_g^{-1}$  or  $1\pi_u^{-2}+\pi_u-\pi_g^*$  character, and complete isomerization on  $S_2$  at  $\sim 90$  fs, a time scale consistent with experimental observation. However, the trajectories with high trans-bending angles on states  $S_3$  and  $S_4$  besides the one shown in Fig. 3(c) end up with C-C fragmentation because of high vibrational energy in the C-C bond and the barrierless character of the potential along this coordinate (see Fig. S6). The branching ratio of the isomerization channel and the kinematically favored C-C symmetric fragmentation channel can be estimated as  $\sim 2 \times 10^{-4}$ . This branching ratio is consistent with the experimental kinetic energy release (KER) spectrum[10].

We further point out that isomerization is possible from the satellite state  $^1\Sigma_u$  ( $S_7$ ) with 3-hole-1-particle (3h1p) electronic character  $1\pi_u^{-2}+\pi_u-\pi_g^*$ . The  $^1\Sigma_u$  state is decayed from the shake-up state  $(C_{1s})^{-1}+\pi_u-\pi_g^*$  in photoionization with Auger energy of 256.8 eV, it crosses with the  $^1\Pi_u$  and  $^1\Pi_g$  states, and can switch to these states that support ultrafast isomerization. Using sudden approximation, we can estimate the  $K$ -shell photionization cross section as  $\sigma \sim \left| \langle \Psi_{M^+}^{N-1} | \hat{a} | \Psi_{M^0}^N \rangle \right|^2$  and determine the ratio of the shake-up state  $(C_{1s})^{-1}+\pi_u-\pi_g^*$  to the  $(C_{1s})^{-1}$  state to be  $\sim 0.03$ .



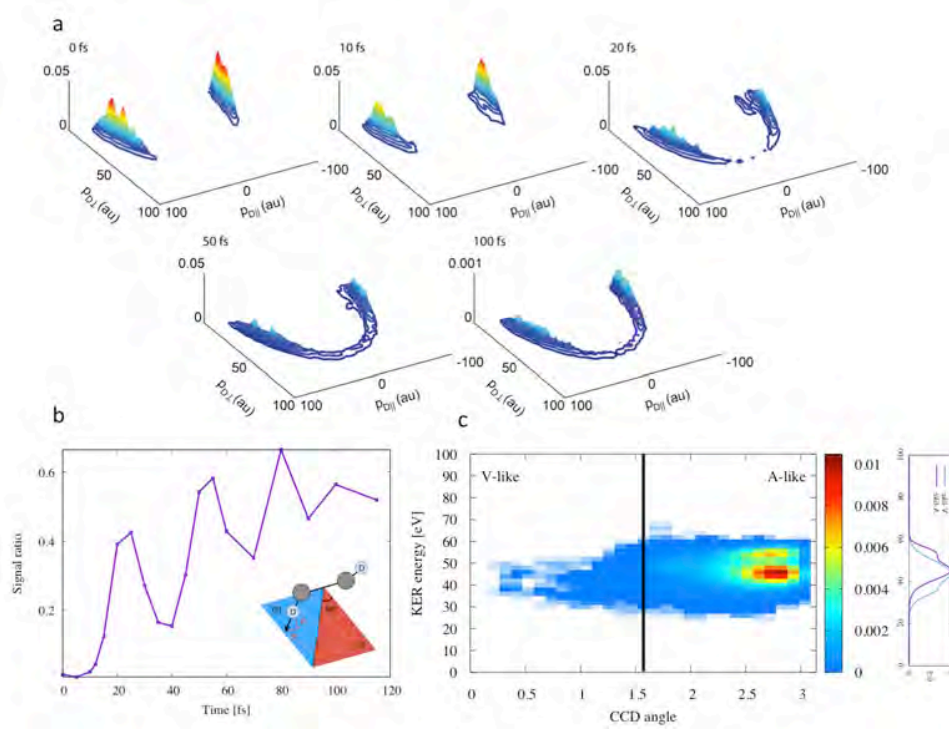


FIG. 4. Simulated Coulomb imaging signal. Temporal evolution of the deuteron momenta from 0 to 100 fs (a). (b) shows signal ratio between region (1) shaded red where  $0^\circ \leq \tan^{-1}(p_{\parallel}/p_{\perp}) < 60^\circ$  and region (2) shaded blue where  $60^\circ \leq \tan^{-1}(p_{\parallel}/p_{\perp}) < 120^\circ$ . (c) The total kinetic energy release (KER) and angle  $\theta$  of distribution of C+/C+/D+/D+ coincidences integrated over all time delays. The CCD angle is defined

$$\text{as } \tilde{\theta} = \cos^{-1} \left( \frac{\text{sgn} \left[ \left( p_{c_a} - p_{c_b} \right) \cdot p_{D_2} \right] \left[ \left( p_{c_a} - p_{c_b} \right) \cdot p_{D_1} \right]}{\left| p_{c_a} - p_{c_b} \right| \left| p_{D_1} \right|} \right), \text{ as the angle a deuteron momentum}$$

makes with the effective C-C axis[10].

In accordance with the experiment[10], we simulated the Coulomb explosion imaging that was used in the experiment to measure the nuclear motion. As shown in Fig. 4(c), the MD trajectories reproduced the vinylidene-like (V-like) signals of  $\theta_{\text{CCD}} < \pi/2$  with a KER below 70 eV, and the general redshift in KER for the V-like channel due to consumption of kinetic energy in trans-bending motion. It is evident that the V-like signals with low KER originate from the higher energy states that have fragmented along the C-C bond after some proton migration. These fragments then continue to rotate after CH<sup>+</sup>+CH<sup>+</sup> symmetric breakup and lead to a V-like signal in the momentum mapping (see Fig. S9)[15]. Thus, while these channels do contain significant hydrogen migration, they do not result in complete isomerization and would not break up into C<sup>+</sup>/CH<sub>2</sub><sup>+</sup> had they not been Coulomb exploded.

An unbroken C-C bond is expected to results in V-like signal with higher KER due to larger Coulomb potential of short C-C distance. To investigate the isomerization



pathway, we take advantage of the fact that Coulomb explosion imaging is sensitive to the actual C-C bond length at the time of tetracation generation. We specifically look at the momentum difference of coincident carbon ions  $p_{C^+C^+} = |p_{C_a^+} - p_{C_b^+}|$ . Using reaction rate theory, we estimate the branching ratio of isomerization channel to be  $2.5 \times 10^{-4}$ [15]. In Fig. 5, we present the momentum difference  $p_{C^+C^+}$  of  $C^+$  ions measured in the time-resolved x-ray pump x-ray probe experiment at Linac Coherent Light Source (LCLS)[10], from which we find the branching ratio of isomerization at 100 fs to be  $\sim 7 \times 10^{-4}$ [15], which is consistent with the here conducted molecular dynamics simulation and reinforces the evidence for the pathways of sub-100 fs isomerization that is only possible due to non-Born-Oppenheimer effect.

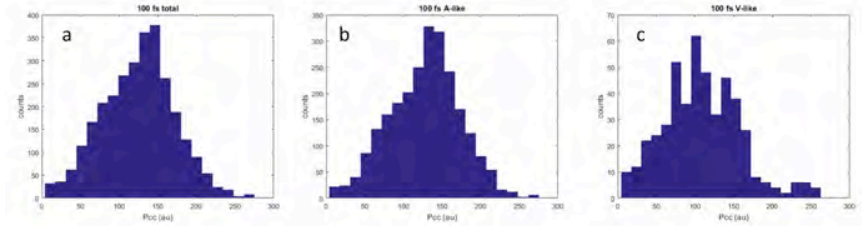


Fig. 5. The measured momentum difference of  $C^+$  ions in the four-particle coincidence Coulomb momentum mapping experiment at 100 fs. (a) Total coincidence counts. (b) coincidence counts of A-like signals. (c) coincidences counts of V-like signals.

In Fig. 4(b), the signal ratio of the simulated Coulomb explosion experiment shows noticeable signature of classical coherence in the bending motion of the acetylene dication. Since the vibrational motion of the acetylene dication is synchronized by the X-ray pump pulses, classical vibration coherence can be expected to occur for 100 fs before dephasing[10]. The vibrational coherence manifests itself in the ratio of deuteron with large bending angles (in region (1), Fig. 4(b)) and in the vicinity of carbon atom (in region (2)). The oscillatory behavior of the ratio from an ensemble of nuclear trajectories simply implies that the vibrational motion is collective.

Our study resolves the debate concerning the physical mechanism of the sub-100 fs isomerization of acetylene dication with a weak C-C bond. We conclude that in fact what appeared as ultrafast isomerization in previous experiments is actually significant proton migration on an excited state that then decays into symmetric breakup. We therefore expect that isomerization, which apparently requires a strong C-C bond to prevent breakup, should occur on the lower lying states and take picoseconds to commence. It is possible for ultrafast isomerization to occur given a soft angular potential on  $1\pi_u^{-1}3\sigma_g^{-1}$  states at the initial phase to reach a high trans-bending angle, and then a bounded potential in C-C stretch coordinate on  $1\pi_u^{-2}$  states to allow the deuteron migrating to the adjacent carbon atom before the C-C bond breakup. However, nonadiabatic couplings are not great enough to make this channel extremely unlikely. Beyond this pathway no isomerization trajectory is

found in the molecular dynamics simulation.

We thank the Hamburg Center for Ultrafast Imaging for financial support. Z. L. thanks the Volkswagen Foundation for support through a Paul-Ewald postdoctoral fellowship, Lee-Ping Wang, Sang-Kil Son, Robin Santra, Mohamed El-Amine Madjet, Kota Hanasaki and Yajiang Hao for assistance.

\*zheng.li@cfel.de

†todd.martinez@stanford.edu

1. Jiang, Y.H., et al., *Ultrafast Extreme Ultraviolet Induced Isomerization of Acetylene Cations*. Physical Review Letters, 2010. **105**: p. 263002.
2. Madjet, M.E.-A., Z. Li, and O. Vendrell, *Ultrafast hydrogen migration in acetylene cation driven by non-adiabatic effects*. The Journal of Chemical Physics, 2013. **138**: p. 094311.
3. Madjet, M.E.-A., O. Vendrell, and R. Santra, *Ultrafast Dynamics of Photoionized Acetylene*. Physical Review Letters, 2011. **107**: p. 263002.
4. Ibrahim, H., et al., *Tabletop imaging of structural evolutions in chemical reactions demonstrated for the acetylene cation*. Nature Communications, 2014. **5**: p. 4422.
5. Jiang, Y.H. and et al., *Ultrafast dynamics in acetylene clocked in a femtosecond XUV stopwatch*. J. Phys. B At. Mol. Opt. Phys., 2013. **46**: p. 164027.
6. Osipov, T., et al., *Photoelectron-Photoion Momentum Spectroscopy as a Clock for Chemical Rearrangements: Isomerization of the Di-Cation of Acetylene to the Vinylidene Configuration*. Physical Review Letters, 2003. **90**: p. 233002.
7. Osipov, T., et al., *Fragmentation pathways for selected electronic states of the acetylene dication*. Journal of Physics B: Atomic, Molecular and Optical Physics, 2008. **41**: p. 091001.
8. Zyubina, T.S., et al., *Theoretical study of isomerization and dissociation of acetylene dication in the ground and excited electronic states*. The Journal of Chemical Physics, 2005. **123**: p. 134320.
9. Duflot, D., J.-M. Robbe, and J.-P. Flament, *Ab initio study of the acetylene and vinylidene dications fragmentation*. The Journal of Chemical Physics, 1995. **102**: p. 355-363.
10. Liekhus-Schmaltz, C.E., et al., *Ultrafast isomerization initiated by X-ray core ionization*. Nat Commun, 2015. **6**: p. 8199.
11. Hishikawa, A., et al., *Visualizing recurrently migrating hydrogen in acetylene dication by intense ultrashort laser pulses*. Phys. Rev. Lett., 2007. **99**: p. 258302.
12. Flammini, R., et al., *Vinylidene dissociation following the Auger-electron decay of inner-shell ionized acetylene*. Phys. Rev. A, 2008. **77**: p. 044701.
13. Matsuda, A., et al., *Visualizing hydrogen atoms migrating in acetylene dication by time resolved three body and four body Coulomb explosion imaging*. Phys. Chem. Chem. Phys., 2011. **13**: p. 8697.
14. B. Gaire, et al., *Photo-double-ionization of ethylene and acetylene near threshold*. Phys. Rev. A, 2014. **89**: p. 013403.
15. Supplemental Materials.
16. Gilbert, A.T.B., N.A. Besley, and P.M.W. Gill, *Self-Consistent Field Calculations of Excited States Using the Maximum Overlap Method*. The Journal of Physical Chemistry A, 2008. **112**: p. 13164-13171.
17. Siegbahn, L., L. Asplund, and P. Kelfve, *The auger electron spectrum of water vapour*. Chem. Phys. Lett., 1975. **35**: p. 330.
18. Tully, J.C., *Molecular dynamics with electronic transitions*. The Journal of Chemical Physics, 1990. **93**: p. 1061-1071.
19. Barbatti, M., R. Shepard, and H. Lischka, p. 415, in *Conical Intersections: Theory, Computation and Experiment*, W. Domcke, D.R. Yarkony, and H. Köppel, Editors. 2011, World Scientific: Singapore.

# SUPPLEMENTAL MATERIAL

## Molecular movie for the isomerization of acetylene dication made by time resolved Coulomb imaging

Zheng Li<sup>1,2,3,\*</sup>, Ludger Inhester<sup>2,3</sup>, Basile Curchod<sup>4</sup>, Chelsea Liekhus-Schmaltz<sup>1,5</sup>, Oriol Vendrell<sup>2,3</sup>, Nikita Medvedev<sup>2,3</sup>, Stefan Pabst<sup>6</sup>, James Cryan<sup>1</sup>, Timur Osipov<sup>1</sup>, Phil Bucksbaum<sup>1,5</sup>, Todd Martinez<sup>1,4,†</sup>

<sup>1</sup>SLAC National Accelerator Laboratory  
2575 Sand Hill Road, Menlo Park, CA 94025, USA

<sup>2</sup>Center for Free Electron Laser Science, Deutsches Elektronen-Synchrotron  
Notkestraße 85, D-22607 Hamburg, Germany

<sup>3</sup>Hamburg Center for Ultrafast Imaging, Luruper Chaussee 149, D-22761 Hamburg, Germany

<sup>4</sup>Department of Chemistry, Stanford University, 333 Campus Drive, Stanford, CA 94305, USA

<sup>5</sup>Department of Physics, Stanford University, 382 Via Pueblo Mall, Stanford, CA 94305, USA

<sup>6</sup>Harvard-Smithsonian Center for Astrophysics, 60 Garden Street, Cambridge, MA 02138, USA

### I. The electronic structure and dynamics of the core-ionized acetylene cation

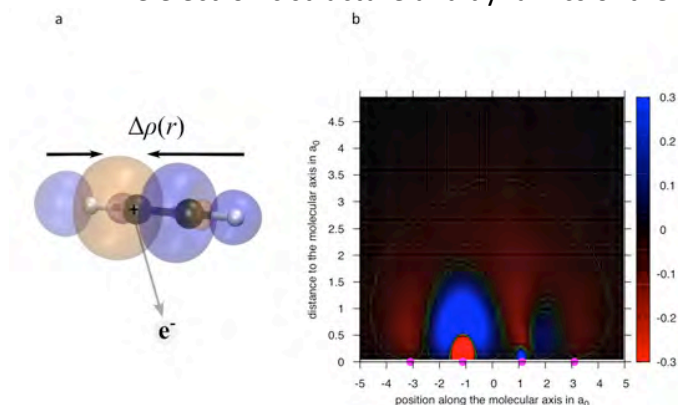


Fig. S1 Electronic screening after core ionization. (a) Sketch of the screening dynamics. The  $C1s$  core hole, as a positive charge, attracts valence electrons in the electronic relaxation after core photoionization. The orange and blue surfaces stand for positive and negative increment in total electron density  $\Delta\rho(\mathbf{r})$  between the fully relaxed electronic structure and that with a pure  $C1s$  core hole in Koopmans' sense. (b) 2D illustration of  $\Delta\rho(r,z)$ , the positions of carbon and deuteron atoms are labeled with dots on the  $x$ -axis, and  $\Delta\rho(r,z) = 2\pi r(\rho_{\text{screen}}(r,z) - \rho_0(r,z))$ .

We treat the electronic structure of the core ionized acetylene cation  $[DCCD]^+$  with a  $\Delta$ SCF method[1]. The electronic potential energies and gradients are computed using GAMESS. In short, a closed-shell Kohn-Sham equation is solved to provide the initial orbitals for  $\Delta$ SCF orbital optimization. The core shell orbitals are then localized on each carbon atoms. A self-consistent field (SCF) procedure then follows with a singly occupied  $C1s$  core orbital. The SCF procedure is carried out with the maximum overlap method, an alternative of *Aufbau* principle to determine orbital occupancies. The occupied orbitals in each new SCF cycle are those that overlap most with the span of the occupied orbitals of previous SCF cycle. The overlap matrix of  $k$ -th SCF cycle is defined as

$$O = (C^{(k)})^\dagger SC^{(k+1)} \quad (0.1)$$

For an orbital  $\phi_i$  in  $(k+1)$ -th SCF cycle, its overlap with the occupation spaces of orbitals in  $k$ -th cycle is defined as

$$p_i^{(n_i)} = \sum_j o_{ij}^{(n_i)}, \quad n_i = 0, 1, 2 \quad (0.2)$$

The occupation of orbitals in  $(k+1)$ -th SCF cycle is then determined by reaching maximal overlap of  $\sum_i p_i^{(n_i)}$ , with  $\sum_i n_i = N_{\text{Electr.}}$ . The dynamic screening effect of valence electrons is shown in Fig. S1, from

the difference of electron density between the converged  $\Delta$ SCF procedure and that from the first SCF cycle. In Fig. S1(b), the electron density difference is illustrated in cylindrical coordinates. The electron screening is essentially equivalent to the build-up of dynamical correlation of electrons in acetylene cation, which involves significant degree of charge transfer and may have an observable effect in transient absorption spectra. We can estimate the time scale of the corresponding shake-up core hole relaxation after core-ionization and build-up of dynamical correlation from the C1s electron binding energy as  $t = 2\pi / E_{1s} \approx 25$  as.

As shown in Fig. S1(a), the net effect of core hole relaxation is the increase of valence bonding electron density in the region of C-C bond, which is attracted by the positively charged core hole. The C-C bond is thus strengthened, and the acetylene cation  $[\text{HCCH}]^+$  has a shorter equilibrium C-C bond length than the neutral acetylene molecule (see Fig. S2(e)). It is also a direct consequence of the valence electron screening effect, that the angular potential along  $\theta_{\text{CCD}}$  coordinate is hardened at shorter C-C bond length  $R_{\text{CC}}$ , because the bonding along C-C axis is strengthened (see Fig. S2(b)), although the angular potential with fixed C-C bond length shows slight softening (see Fig. S2(c) and (d)).

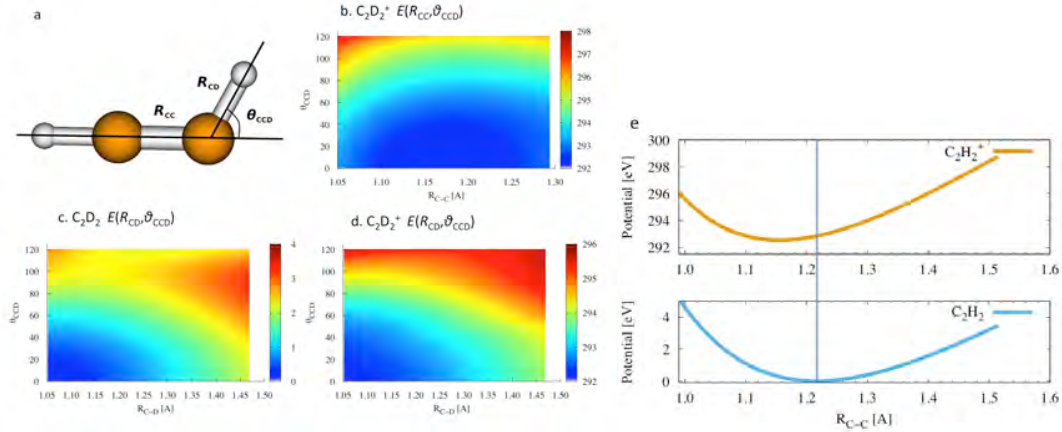


Fig. S2 The potential of the C1s core ionized acetylene cation ( $^2\Sigma$  state). (a) Illustration of the coordinates  $R_{\text{CC}}$ ,  $R_{\text{CD}}$  and  $\theta_{\text{CCD}}$ . (b) 2D potential  $E(R_{\text{CC}}, \theta_{\text{CCD}})$  of core ionized acetylene cation with  $R_{\text{CD}} = 1.06 \text{ \AA}$ . (c) 2D potential  $E(R_{\text{CD}}, \theta_{\text{CCD}})$  of neutral acetylene molecule on  $^1\Sigma_g$  state with  $R_{\text{CC}} = 1.22 \text{ \AA}$ . (d) 2D potential  $E(R_{\text{CD}}, \theta_{\text{CCD}})$  of core ionized acetylene cation on  $^2\Sigma$  state with  $R_{\text{CC}} = 1.22 \text{ \AA}$ . (e) 1D potential  $E(R_{\text{CC}})$  of core ionized acetylene cation on  $^2\Sigma$  state with  $R_{\text{CD}} = 1.06 \text{ \AA}$  and  $D_{\infty h}$  symmetry.

## II. Auger decay and generation of acetylene dication



From the simulated Auger spectra, we could determine the FWHM of the experimental spectra to be  $\sim 2.5\text{eV}$ [3]. In the coincidence experiment[9], the Auger electrons that correlated with the isomerization channel have a distribution centered at  $255.5\text{ eV}$  [9], the Auger electrons could have three sources, from the low energy wing of the  $1\pi_u^{-2}$  states ( $^1\Delta_g$ ,  $^1\Sigma_g$ ) centered at  $257.1\pm 0.2\text{eV}$ , from the high energy wing of the  $1\pi_u^{-1}3\sigma_g^{-1}$  states ( $^1\Pi_u$ ) centered at  $252.6\pm 0.4\text{eV}$ , and from the  $3\text{h}1\text{p}$  satellite state ( $^1\Sigma_u$ ) with Auger energy of  $256.8\text{ eV}$ . The pathways on the  $^1\Pi_u$  and  $^1\Sigma_u$  states support ultrafast isomerization on the sub-100 fs time scale[10], and the pathways on the  $^1\Delta_g$  and  $^1\Sigma_g$  states are open for isomerization on a longer time scale that corresponds to the dynamics of potential barrier crossing. These channels all together contribute to the measured vinylidene-like signals in Ref. [9, 11].

For dynamical Auger spectra, we adopt the single determinant  $\Delta\text{SCF}$  method for the saving of computational cost. The Auger spectra show dominant decay channels into singlet states, and a cumulative Auger lifetime of  $\sim 8\text{ fs}$ . Within the Auger lifetime, it is sufficient for the geometrical relaxation to take place on the cationic  $^2\Sigma$  state, that the acetylene cation evolves towards a linear structure with shorter C-C bond length. The Auger rates computed at each step along the trajectories are used to construct initial conditions of dynamics of dications through kinetic rate equation.

### III. Dynamics on the dicationic states and Coulomb explosion imaging

#### IIIA. Dicationic potentials

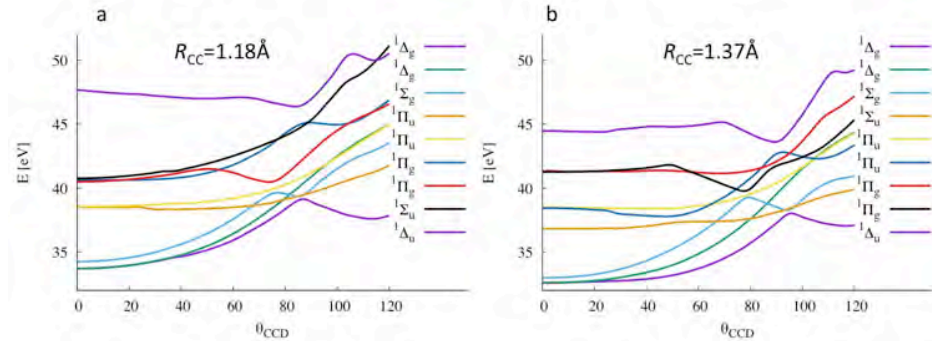


Fig. S4 1D diabatic potentials  $E(\theta_{\text{CCD}})$  of acetylene dication on the CASSCF(8,8)/6-31G\* level, with  $R_{\text{CD}}=1.12\text{\AA}$  and  $R_{\text{CD}}=1.18\text{\AA}$ ,  $1.37\text{\AA}$ , i.e. the C-C bond lengths of the Franck-Condon geometry and the equilibrium CC bond length of dicationic ground states. The electronic characters are labeled by the representations correlated with that of linear geometry ( $\theta_{\text{CCD}}=0^\circ$ ,  $D_{\infty h}$  symmetry). At the Franck-Condon geometry, the  $^1\Delta_g$  and  $^1\Sigma_g$  states that correlate with adiabatic states  $S_0$ - $S_2$  are of  $1\pi_u^{-2}$  character, the  $^1\Pi_u$  and  $^1\Pi_g$  states that correlate with adiabatic states  $S_3$ - $S_4$  are of electronic character  $1\pi_u^{-1}3\sigma_g^{-1}$  and  $1\pi_u^{-1}2\sigma_u^{-1}$ . The  $^1\Sigma_u$  state is a 3-hole-1-particle (3h1p) satellite state with electronic character  $1\pi_u^{-2}+(\pi_u \rightarrow \pi_g^*)$ , it correlates initially with  $S_7$  at Franck-Condon geometry (a), and becomes  $S_3$  as the CC bond stretches (b).

The electronic structure of acetylene dication is solved for fewest-switches surface hopping molecular dynamics on the CASSCF(8,8)/6-31G\* level, which gives quantitatively consistence potential on the CASPT2(8,10)/6-31G\* level. In Fig. S4, we present the diabatic potential of the dication along the trans-bending coordinate  $\theta_{\text{CCD}}$ . The potential curve of  $^1\Sigma_u$  state cuts through that of  $^1\Pi_g$  and  $^1\Pi_u$  states as C-C bond stretches (Fig. 1). The  $^1\Sigma_u$ ,  $^1\Pi_g$  and  $^1\Pi_u$  states together form a pathway for isomerization with low barrier in the corresponding adiabatic states.



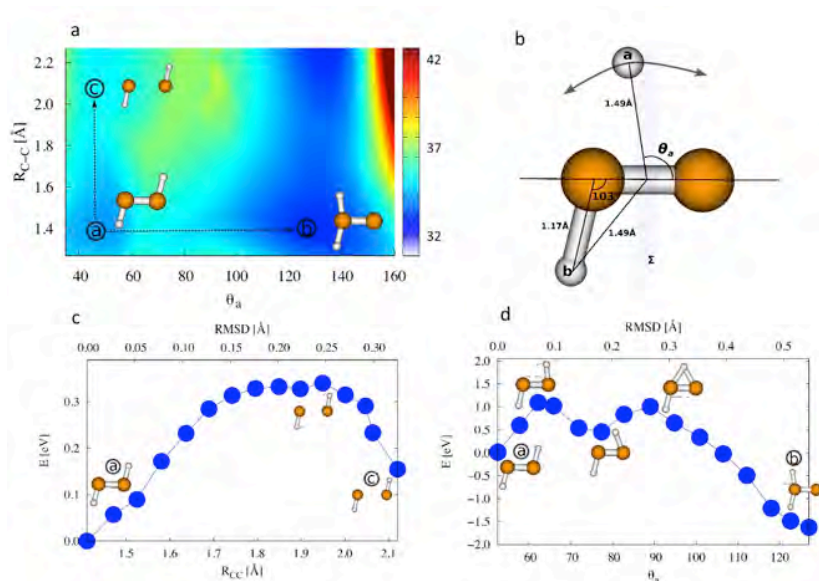


Fig. S5 Isomerization pathway on an  $1\pi_u^{-2}$  state  $S_2$ , that is crucial to complete the isomerization when the dication that decays from  $1\pi_u^{-1}3\sigma_g^{-1}$  states. (a) 2D potential  $E(R_{CC}, \theta)$  from scan with rigid geometry on the remaining degrees of freedom. (b) Illustration of degrees of freedom for rigid potential scan in (a), deuteron  $D_b$  is fixed at the position from optimized geometry of  $[CD_2C]^{2+}$ . (c) Potential along C-C fragmentation pathway with relaxed geometry. (d) Potential along isomerization pathway with relaxed geometry.

In Fig. S5, we present the potential along C-C fragmentation and isomerization pathways on an  $1\pi_u^{-2}$  state  $S_2$ , which is crucial to complete isomerization process by providing a bounded C-C potential for the dication. We optimize the geometry on the excited dicationic states for the isomerized and fragmented dication, and calculate the potential along the isomerization and fragmentation coordinates. Fig. S5(c) shows bounded potential for C-C stretch coordinate with a barrier of  $\sim 0.3$  eV, and in Fig. S5(d), we found signature that isomerization requires formation of triangular C-D-C bridge as the deuteron migrates halfway to the middle of the two carbon atoms, with the two carbon atoms contracting towards each other. This however imposes another disadvantageous factor to the isomerization channel, because the C-C stretch motion is kinematically enhanced due to kinetic energy release from geometric relaxation after Auger decay.

### IIIB. Dynamics of dication

The recoil momentum of outgoing Auger electron with energy of ca. 255 eV and the angular momentum of the trans-bending motion can set the  $[C_2D_2]^{2+}$  dication into rotation, the rotation has been used as a clock to estimate the time of isomerization[11]. We show in Fig. S6 the rotational motion of the C-C axis from the molecular dynamics simulation. The existence of rotation is consistent with the previous literature, however the dications only rotate for  $\sim 0.15$  rad in 100 fs, slower than expected in Ref. [11], and the dispersion of the  $\theta_{CC}$  angle distribution also shows a deceleration. Because the C-C bond stretches from  $1.21\text{\AA}$  to  $1.37\text{\AA}$ , and the angular velocity  $\omega$  decelerates due to conservation of angular momentum. Besides, the recoil momentum of Auger electron of 255 eV adds kinetic energy of maximal  $\sim 0.012$  eV to the bending motion of the dication when it acts vertically to the C-C axis. The recoil motion has very limited influence to isomerization in comparison with the total kinetic energy of 0.95 eV, especially it is hard to compete with for C-C stretching motion of 0.43 of kinetic energy that supports the symmetric fragmentation channel. For the lowest three singlet states without ionization from  $\sigma$ -orbital, the unidirectional  $\sigma$ -bond along the C-C axis should weaken the effect of recoil momentum to support isomerization. Besides, the Auger electron from delocalized valence orbitals should in fact impose recoil momentum to all atoms, it could also weaken the effect of the supporting effect to isomerization. Thus we suggest that the



isomerization due to barrier crossing on the lower  $1\pi_u^{-2}$  dicationic state takes place at much longer time scales, and it is consistent with the conclusion from energetics perspective in Ref. [12]

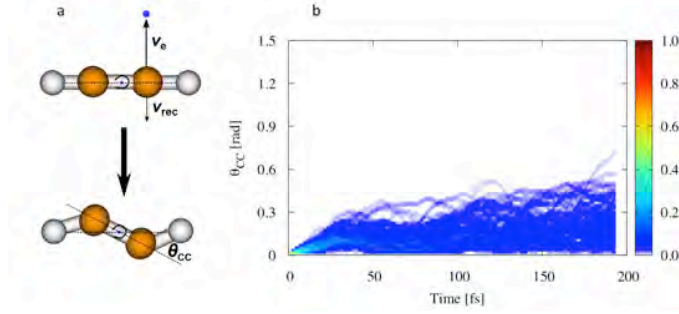


Fig. S6 (a) Sketch of rotation of C-C axis with initial velocity  $v_{rec}$  due to recoil momentum of Auger electron with velocity  $v_e$  on the lever, and possible supporting effect the C-C rotational motion to isomerization. (b) Rotation of C-C axis in the lab system due to recoil momentum of Auger electron, calculated from molecular dynamics simulation, where the rotation angle is defined as

$$\theta_{cc}(t) = \left| \cos^{-1} \left( \frac{\vec{R}_{cc}(t) \cdot \vec{R}_{cc}(0)}{|\vec{R}_{cc}(t)| |\vec{R}_{cc}(0)|} \right) \right|.$$

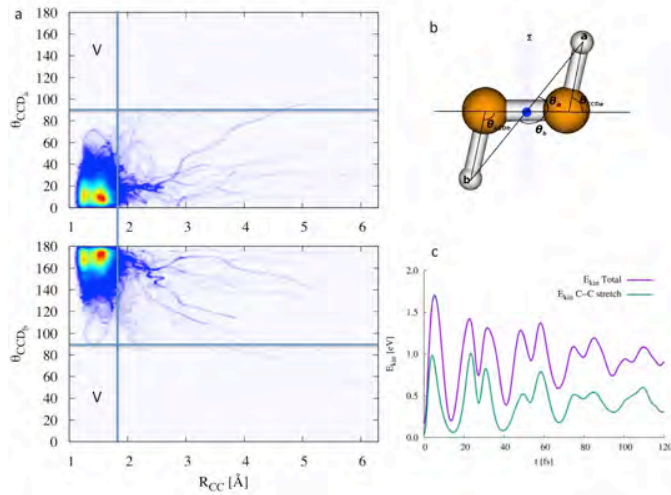


Fig. S7 Dynamics of the acetylene dication after Auger decay. (a)  $(\theta_{ccd}, R_{cc})$  accessed by the ensemble of nuclear trajectories from fewest-switches surface hopping simulation. Regions for V-like configurations are labeled for  $\theta_{ccd} \geq \pi/2$  and  $R_{cc} \leq 1.8 \text{ \AA}$ . (b) Illustration of angular coordinates  $\theta_{ccda}$  and  $\theta_{ccdb}$ . (c) Time evolution of total kinetic energy of the dication and the kinetic energy distributed in the C-C stretch coordinate.

In Fig. S7, we present  $(\theta_{ccd}, R_{cc})$  that can be accessed by the ensemble of nuclear trajectories from fewest-switches surface hopping simulation, from which no isomerization channel can be detected. Fig. 7(c) shows the kinetic energy distribution in the C-C stretch and the rest 5 degrees of freedom. Because both C-C stretch and trans-bending motion are quasi barrier free on the  $1\pi_u^{-1}3\sigma_g^{-1}$  states, we can assume all the occupied states of these two degrees of freedom correspond to open channels. We can estimate the branching ratio between C-C fragmentation and isomerization simply from

probability of open channels  $P_i = \frac{(2\pi m_i kT)^{3/2} V}{h^3} e^{-\frac{E_i}{kT}}$ . Assume ambient temperature  $T=300 \text{ K}$ , the kinetic

energy of C-C stretch is found for the 120 fs dynamics as  $\frac{1}{T} \int dt E_{KER, CC}(t) \sim 0.43 \text{ eV}$ , and

$\frac{1}{T} \int dt E_{\text{KER}}(t) \sim 0.95$  eV, for the trans-bending (TB) motion we assume all recoil energy of 0.012 eV is pumped into this degree of freedom (DOF) and the rest is equally distributed in the five DOFs, we have  $E_{\text{KER,TB}} \sim \frac{2}{5} \times (0.52 - 0.012) + 0.012 = 0.215$  eV. The ratio between the V- and A-like channels is estimated to be  $2.5 \times 10^{-4}$ . It is consistent with the estimated experimental value of  $\sim 7 \times 10^{-4}$ .

### IIIC. Coulomb momentum mapping

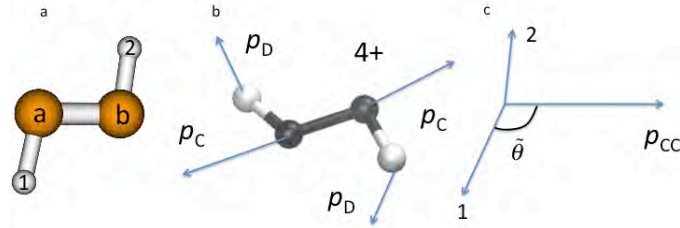


Fig. S8 Schematic illustration of Coulomb momentum mapping from  $[\text{C}_2\text{D}_2]^{4+}$  induced by the X-ray probe pulses.

The Coulomb momentum mapping by further core photoionization and Auger decay with an X-ray probe pulse of certain time delay produces a tetracation  $[\text{C}_2\text{D}_2]^{4+}$ . The Coulomb explosion of the tetracation is simulated by a classical Hamiltonian of four singly charged particles  $\text{C}^+/\text{C}^+/\text{D}^+/\text{D}^+$

$$H = T + V_{\text{Coul}}(r_1, r_2, r_a, r_b) \quad (0.7)$$

$$V_{\text{Coul}}(r_1, r_2, r_a, r_b) = \frac{1}{r_{1a}} + \frac{1}{r_{1b}} + \frac{1}{r_{2a}} + \frac{1}{r_{2b}} + \frac{1}{r_{12}} + \frac{1}{r_{ab}},$$

because dynamics of the highly repulsive tetracation is not sensitive to its actual electronic structure, where  $T$  is the kinetic energy,  $r_1, r_2, r_a, r_b$  are the coordinates of the carbon and deuterium ions as shown in Fig. S8(a), and  $V_{\text{Coul}}(r_1, r_2, r_a, r_b)$  is the Coulomb potential. Molecular dynamics of tetracation  $[\text{C}_2\text{D}_2]^{4+}$  is carried out for 250 fs. Final distances of ions are of  $\sim 100 \text{ \AA}$ , from which we can assume the Coulomb potential has been fully released. The deuteron momenta are projected to the C-C axis defined by the difference of momenta of the two carbon ions. To classify the four-particle coincidences signal, we define the angle  $\tilde{\theta}$  [10]

$$\tilde{\theta} = \cos^{-1} \left( \frac{\text{sgn}[(p_{c_a} - p_{c_b}) \cdot p_{d_2}] [(p_{c_a} - p_{c_b}) \cdot p_{d_1}]}{|p_{c_a} - p_{c_b}| |p_{d_1}|} \right). \quad (0.8)$$

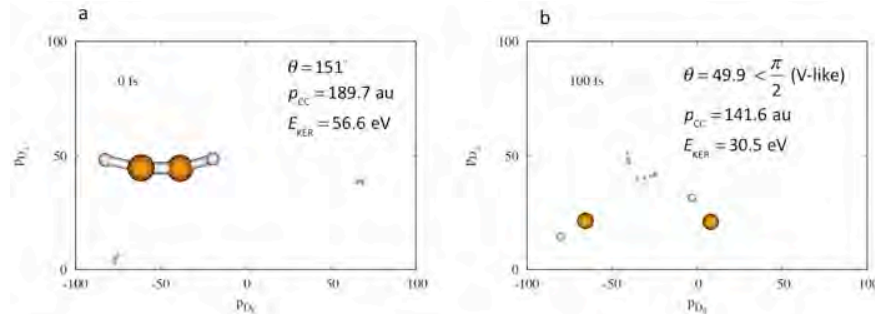


Fig. S9 Simulated Coulomb momentum mapping from a representative trajectory with time delay of X-ray probe pulses (a)  $t=0$  fs (b)  $t=100$  fs. The trajectory gives V-like signal at time delay  $t=100$  fs, belongs however to the C-C fragmentation channel. The  $\text{CD}^+$  ion fragment carries remnant angular momentum

inherited from trans-bending motion before fragmentation. For each time delay  $t$ , we compute five deuteron momentum mappings from  $t-2$  to  $t+2$  fs.

We classify the  $C^+/C^+/D^+/D^+$  four-particle-coincidence as ‘vinylidene-like’ (V-like) for  $\tilde{\theta} < \frac{\pi}{2}$ , such that both deuteron momenta reside on the same side of the bisection plane that divides the C-C axis. The remaining coincidences with  $\tilde{\theta} > \frac{\pi}{2}$  are referred as ‘acetylene-like’ (A-like) with deuteron momenta on opposite sides of the bisection plane. However, V-like coincidence does not necessarily correspond to an isomerization event.

Assuming a C-C bond length limit of dissociation to be 1.5 Å, and considering only the collinear Coulomb force between the two  $C^+$  ions, an isomerized acetylene dication should give  $p_{C^+C^+}$  with a lower bound of  $\sim 181$  au and V-like signal in the four-particle momentum map. Because the  $C^+$  ions also feel the Coulomb force from the  $D^+$  ions, the actually  $p_{C^+C^+}$  should be higher than 181 au. In the non-isomerized trajectories of the molecular dynamics calculation that satisfy the lower bound, the lowest  $\tilde{\theta}$  angle they can reach is  $22^\circ$ , with  $p_{C^+C^+} = 199$  au. In the V-like signals of Fig. 5, we attribute the four-particle coincidence signals with  $\tilde{\theta} \leq 22^\circ$  and  $p_{C^+C^+} \geq 199$  au to the isomerization channel, from this consideration we find its branching ratio to be  $\sim 7 \times 10^{-4}$ .

In Fig. S9, we show a representative trajectory of symmetric fragmentation channel with breakup of C-C bond, which gives V-like coincidence signal due to the remnant angular momentum of the  $CD^+$  fragments. However, the C-C fragmented trajectory with V-like coincidence should have lower KER and  $p_{CC}$ , and can be distinguished from isomerization channel with V-like coincidence, because long C-C distance simply implies low Coulomb potential release. Thus, we reconsider the measured Carbon momenta in the experiment with respect to the C-C momentum. Fig. S10 and S11 show the momentum difference obtained in the experiment and from the MD simulations.

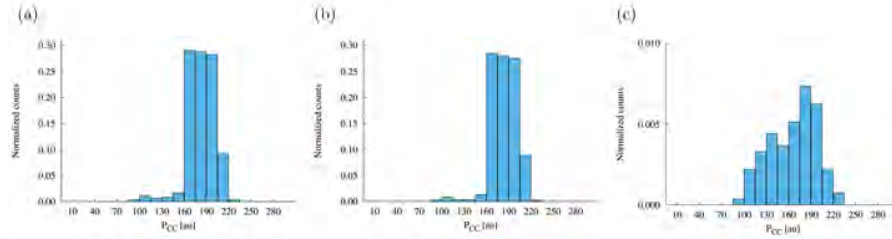


Fig. S10. Momentum difference of  $C^+$  ions in the Coulomb momentum mapping at 100 fs from molecular dynamics calculations. (a) Total coincidence counts. (b) Coincidence counts of A-like signals. (c) Coincidence counts of V-like signals.

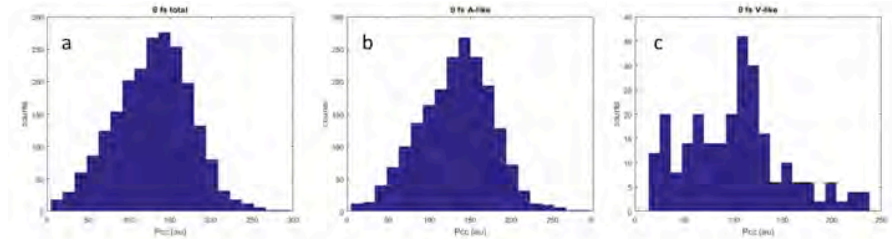


Fig. S11. The measured momentum difference of  $C^+$  ions in the Coulomb momentum mapping at 0 fs. (a) Total coincidence counts. (b) coincidence counts of A-like signals. (c) coincidences counts of V-like signals.

It is noticeable that there are coincidence counts in Fig. 5 with low momentum difference  $p_{c^+c^+} \leq 70$  au that appear within 100 fs, these coincidence counts are not found in the molecular dynamics simulation of 120 fs, and they correspond to C-C distance larger than 30 Å, these coincidence count signals may come from the highly dissociative states above  $S_7$ , which we have not considered in the simulation and should also have negligible contribution to isomerization. Especially, the coincidence counts with very low momentum difference down to 10 au appear from 0 fs (Fig. S11), these signals correspond to C-C distances that could be larger than 1 μm, and are comparable to the size of the XFEL-sample interaction region of 50 μm<sup>2</sup> [10]. They give a clear hint that despite of the filtering using momentum conservation criterion,  $|p_{d_{1,j}} + p_{d_{2,j}} + p_{c_{1,j}} + p_{c_{2,j}}| = p_j < \delta p_j, j = x, y, z$  in the lab system [10], a part of coincidence counts of Coulomb momentum mapping may arise from  $C^+D^+$  fragments of two distant  $C_2D_2^{2+}$  dications instead of a same parent cation, these accidental coincidences should be further filtered out from the dataset in order to have a clean interpretation of the Coulomb momentum mapping experiment for the making of molecular movie. For improving interpretation of Coulomb momentum mapping technique, we thus propose an additional criterion to ensure that the coincidence counts are originated from fragments of the same parent ion by filtering out the coincidence with relative momentum of two ion particles which are too low than that are allowed by reasonable bond length between these two particles in their parent ion. This novel criterion basically reflects the essence of Coulomb explosion imaging of bond length.

\*zheng.li@cfel.de

†todd.martinez@stanford.edu

1. Gilbert, A.T.B., N.A. Besley, and P.M.W. Gill, *Self-Consistent Field Calculations of Excited States Using the Maximum Overlap Method*. The Journal of Physical Chemistry A, 2008. **112**: p. 13164-13171.
2. Inhester, L., et al., *Auger spectrum of a water molecule after single and double core ionization*. The Journal of Chemical Physics, 2012. **136**(14): p. 144304.
3. Kivimäki, A., et al., *Angle-resolved Auger spectra of the C<sub>2</sub>H<sub>2</sub> molecule*. Journal of Physics B: Atomic, Molecular and Optical Physics, 1997. **30**: p. 4279.
4. Manne, R. and H. Ågren, *Auger transition amplitudes from general many-electron wavefunctions*. Chemical Physics, 1985. **93**: p. 201-208.
5. Siegbahn, L., L. Asplund, and P. Kelfve, *The auger electron spectrum of water vapour*. Chem. Phys. Lett., 1975. **35**: p. 330.
6. Chen, M.H., F.P. Larkins, and B. Crasemann, *Auger and Coster-Kronig radial matrix elements for atomic numbers 5<Z<93*. Atomic Data and Nuclear Data Tables, 1990. **45**: p. 1.
7. Son, S.-K., L. Young, and R. Santra, *Impact of hollow-atom formation on coherent x-ray scattering at high intensity*. Physical Review A, 2011. **83**: p. 033402.
8. Inhester, L., et al., *Auger spectrum of a water molecule after single and double core ionization*. The Journal of Chemical Physics, 2012. **136**: p. 144304.
9. Osipov, T., et al., *Fragmentation pathways for selected electronic states of the acetylene dication*. Journal of Physics B: Atomic, Molecular and Optical Physics, 2008. **41**: p. 091001.
10. Liekhus-Schmaltz, C.E., et al., *Ultrafast isomerization initiated by X-ray core ionization*. Nat Commun, 2015. **6**: p. 8199.
11. Osipov, T., et al., *Photoelectron-Photoion Momentum Spectroscopy as a Clock for Chemical Rearrangements: Isomerization of the Di-Cation of Acetylene to the Vinylidene Configuration*. Physical Review Letters, 2003. **90**: p. 233002.
12. Zyubina, T.S., et al., *Theoretical study of isomerization and dissociation of acetylene dication in the ground and excited electronic states*. The Journal of Chemical Physics, 2005. **123**: p. 134320.